

2 **Modeling The Nutrientsbehavior in Intervertebral Discs:** 3 **A Boundary Integral Simulation**

4 **Y. González*, F. Nieto¹ and M. Cerrolaza^{1†}**

5 **Abstract:** It is a well-known fact that computational biomechanics and mechanobi-
6 ology have deserved great attention by the numerical-methods community. Many
7 efforts and works can be found in technical literature. This work deals with the
8 modeling of nutrients and their effects on the behavior of intervertebral discs. The
9 numerical modeling was carried out using the Boundary Element Method (BEM)
10 and an axisymmetric model of the disc. Concentration and production of lactate and
11 oxygen are modeled with the BEM. Results agree well enough with those obtained
12 using finite elements. The numerical efforts in the domain and boundary discretiza-
13 tions are minimized using the BEM. Also, the effect of the calcification of the disc
14 that causes the vascularization loss has been studied. The glucose, oxygen and lac-
15 tate components behavior has been analyzed applying a mixed loading-unloading
16 process, then allowing the study of the disc-height variations due to the degradation
17 of the disc.

18 **Keywords:** Mass transport, nonlinear diffusion, boundary integral analysis, in-
19 tervertebral discs.

20 **1 Introduction**

21 Computational biomechanics and mechanobiology have deserved great attention by
22 the numerical-methods community. Many works can be cited, applied to study the
23 biological tissue response like bone [1, 2], thermal influence on tissues [3], bone re-
24 modeling [4] and mass-transport phenomena in the intervertebral disc [5, 6]. These
25 simulations were implemented on both, finite element (FEM) and boundary ele-
26 ment (BEM) frameworks under different considerations. In particular, Ferguson et
27 al [6] included the analysis of the convective term caused by the effect of loading on
28 the velocity field. Meanwhile, Mokhbi et al [7] reported results regarding factors

* National Institute for Bioengineering, Central University of Venezuela, Caracas, Venezuela

† International Center for Numerical Methods in Engineering, Polytechnic University of Catalonia, Barcelona, Spain

affecting the intervertebral disc nutrition by evaluating the concentration of oxygen, glucose and lactic acid. Their results provided good examples to validate our boundary integral approach. On the other hand, recent advances in boundary element techniques also show suitable formulations for solving time-dependent terms in the only-boundary sense. These techniques, like the Dual Reciprocity Method (DRBEM, [8], have been previously implemented within linear poroelasticity [9]) and diffusion-convection-reaction analyses [10]. Boundary Integral Methods advantages also involve high accuracy solutions at both boundary and internal points and good performance solving the coupled equations system for multiple regions [8, 11, 12]. More recently, González et al [13] proposed a poroelastic axisymmetric boundary element callus model to characterize bone tissue properties using strain/stress fields as mechanical stimuli affecting cell differentiation and ossification pathway.

Most of the reported work in literature has been done using the finite element method. Galbusera et al [14] have discussed and compared 4 FEM-based methods for modeling swelling in intervertebral discs. Kima et al [15] presented an inverse method to study the tissue mechanics, using eigenvectors and eigenvalues to help in the required mathematical work. The work of Yao & Gu [16] presented a finite element analysis of inhomogeneous domains to deal with solute transport in vertebral discs. Zhu et al [17] also discussed a FE model to simulate the dynamical conditions and nutritional transport in intervertebral discs. Hubbard & Byrne [18] addressed the multiphase tumor growth using a continuous mathematical model. Isaksson et al [19] have presented a two dimensional FE-adaptive model, together with a statistical approach, for simulating the fracture and tissue growing in long-bone fractures.

However, when looking at the boundary integral methods, little work can be found. We can mention the work of Ochiai & Takeda [20] who presented a BEM approach to simulate the diffusion-convection by using a meshless method. The two dimensional modeling of cell adhesion is presented in a paper by Jiang & Yang [21]. These authors formulated the problem using a coupled between a FE-model for the cell and a BE-model for the substrate. On their side, Haider & Guilak [22] have used a BEM formulation in the Laplace transform domain to model stresses in a cartilage.

Other approaches recently explored are the lattice methods. A lattice approach was employed by Checa & Prendergast [23] for modeling the interaction between a scaffold and tissue formation with a mechanobiological model.

In this paper, a coupled nonlinear mass-transport model defined by diffusion-reaction equations was implemented using the boundary element method to simulate the cells behavior following the FEM works by Mokhbi et al [7] and [5]. A mixed nu-

merical analysis was used to simulate the effect of loading, diffusion coefficient and solute size on the response of each nutrient individually. A complete description of nutrients distribution is also modeled. The Dual Reciprocity Method (DRBE-M) was included to deal with domain terms, while the integration of both regular and singular kernels were performed following a mixed scheme [24]. Additional terms of new equations were approximated according to Bai & Lu [25] in diffusion problems and following Park & Banerjee [9] in linear poroelasticity. Multiregion models were also considered. The results show the capability of the Boundary Integral Methods to simulate problems in biomechanics. Other testing models such as heat transfer o contaminant concentration have also been used to verify the DRBE-M code versatility.

2 Materials and Methods

2.1 A summary of the Boundary Element Method

A time domain boundary element method (BEM) for axisymmetric poroelasticity was employed to characterize bone tissue properties using strain/stress fields as mechanical stimuli affecting cell differentiation and ossification pathway [13]. The poroelasticity theory [26] is show below in equation (1) as well as the classic boundary integration equation (2):

$$(\lambda + \mu)u_{j,ij} + \mu u_{i,jj} - \beta p_{,i} + f_i = 0 \quad (1a)$$

$$kp_{,jj} - \left(\frac{\beta^2}{\lambda_u - \lambda} \right) \dot{p} - \beta \dot{u}_{j,j} + \psi = 0 \quad (1b)$$

$$C_{ij}U_i(P) = 2\pi \int_{\Gamma} U_{ij}^*(P, Q) T_j(Q) r(Q) d\Gamma - 2\pi \int_{\Gamma} T_{ij}^*(P, Q) U_j(Q) r(Q) d\Gamma + \int_{\Omega} U_{ij}^*(P, Q) B_j(P, t) d\Omega \quad (2)$$

where u_r , u_z and p represent the displacement field and pore pressure respectively. T_r , T_z are the tractions and q is the fluid flow. U_{ij}^* and T_{ij}^* denote the fundamental solutions for steady-state poroelasticity [11], f_i are the body forces, B_j stores the displacement/pressure gradients and the time terms. λ and μ are the drained Lamé's elastic constants, λ_u is the undrained elastic modulus, k is the permeability and β is a function of B , called the compressibility coefficient or Skempton pore-pressure coefficient.

Bone healing also requires to simulate how the stimuli can affect the bone cell evolutions. However, the Biot's diffusion-deformation model (equation 1.b) consists

in a Laplace equation governing the pore pressure. Nevertheless, in spite of its relatively simple form, analogies with mass and charge transport phenomena, [27, 28] and heat distribution problems [3] have been implemented to simulate the rate of change of solute/cell densities [2, 7, 6]. Here, classical balance laws led to a generalized formulation of diffusion-convection-reaction equation to solve the unknown scalar field $c(x, t)$ described in equation (3)

$$D\nabla^2 c - v \cdot \nabla c - \phi(c) = \frac{dc}{dt} \quad (3)$$

88 where $c(x, t)$ is the cell/solute density, D is the diffusion coefficient, v is the velocity
89 field and $\phi(c)$ is the reactive term.

According to (2), BEM capabilities lead to accurate solution to be obtained efficiently, but, the approximation of domain terms remains limited. In this sense, DRBEM let us to obtain approximate functions for those terms to be integrated at the only-boundary sense. Thus, gradients and time-derivatives terms written in equations (1) and (3) can now be treated with this technique. A set of particular solutions of equation (1) can be approximate by using global shape functions (4).

$$p(x) = \sum_{n=1}^{\infty} \int_0^{2\pi} S(x, \xi_n) d\theta \beta(\xi_n) \quad (4a)$$

$$\dot{u}_l(x) = \sum_{n=1}^{\infty} \int_0^{2\pi} D_{ij}(x, \xi_n) d\theta \dot{\beta}_j(\xi_n) \quad (4b)$$

$$\dot{p}(x) = \sum_{n=1}^{\infty} \int_0^{2\pi} K_k(x, \xi_n) d\theta \dot{\beta}(\xi_n) \quad (4c)$$

$$u_j^p(x) = \sum_{n=1}^{\infty} \int_0^{2\pi} U_j(x, \xi_n) d\theta \beta(\xi_n) \quad (4d)$$

$$\sigma_{ij}^p(x) = \sum_{n=1}^{\infty} \int_0^{2\pi} S_{ij}(x, \xi_n) d\theta \beta(\xi_n) \quad (4e)$$

$$t_j^p(x) = \sum_{n=1}^{\infty} \int_0^{2\pi} T_j(x, \xi_n) d\theta \beta(\xi_n) \quad (4f)$$

$$p^p(x) = \sum_{n=1}^{\infty} \int_0^{2\pi} P_j(x, \xi_n) d\theta \dot{\beta}_j(\xi_n) + \int_0^{2\pi} P_k(x, \xi_n) d\theta \dot{\beta}_k(\xi_n) \quad (4g)$$

$$q^p(x) = \sum_{n=1}^{\infty} \int_0^{2\pi} Q_j(x, \xi_n) d\theta \dot{\beta}_j(\xi_n) + \int_0^{2\pi} Q_k(x, \xi_n) d\theta \dot{\beta}_k(\xi_n) \quad (4h)$$

where $u_i^p y t_i^p$ are defined

$$\{u_i^p\} = \{u_r^p \quad u_z^p\} y \{t_i^p\} = \{t_r^p \quad t_z^p\}$$

Additionally after to approximate the boundary the equations (4. a-h) can be written

$$\{P\} = [S]\{\beta\} \quad (5a)$$

$$\{u_i^p\} = [U_i]\{\beta\} \quad (5b)$$

$$\{t_i^p\} = [T_i]\{\beta\} \quad (5c)$$

$$\{P^p\} = [P_k P_p] \begin{Bmatrix} \dot{\beta}_k \\ \dot{\beta}_p \end{Bmatrix} \quad (5d)$$

$$\{Q^p\} = [Q_k Q_p] \begin{Bmatrix} \dot{\beta}_k \\ \dot{\beta}_p \end{Bmatrix} \quad (5e)$$

$$\begin{Bmatrix} \dot{u}_k \\ \dot{P} \end{Bmatrix} = \begin{bmatrix} D_{kj} & 0 \\ 0 & K_P \end{bmatrix} \begin{Bmatrix} \dot{\beta}_j \\ \dot{\beta}_P \end{Bmatrix} \Rightarrow \begin{Bmatrix} \dot{\beta}_j \\ \dot{\beta}_P \end{Bmatrix} = \begin{bmatrix} D_{jk}^{-1} & 0 \\ 0 & K_P^{-1} \end{bmatrix} \begin{Bmatrix} \dot{u}_k \\ \dot{P} \end{Bmatrix} \quad (5f)$$

90

Then the equation (1) can be written in matrix form, in order to be solved by a suitable time-integration scheme

$$\begin{bmatrix} G_{ij} & 0 \\ 0 & G_{kk} \end{bmatrix} \begin{Bmatrix} t_j \\ q \end{Bmatrix} - \begin{bmatrix} H_{ij} & M_{ik} \\ 0 & H_{kk} \end{bmatrix} \begin{Bmatrix} u_j \\ p \end{Bmatrix} = \begin{bmatrix} 0 & 0 \\ M_{kj} & M_{kk} \end{bmatrix} \begin{Bmatrix} \dot{u}_j \\ \dot{p} \end{Bmatrix} \quad (6)$$

where

$$[M_{ik}] = ([G_{ij}][\hat{T}_j] - [H_{ij}][\hat{U}_j])[S] - 1$$

$$[M_{ki} \quad M_{kk}] = ([G_{kk}][\hat{Q}_s \quad \hat{Q}_k] - [H_{kk}][\hat{P}_s \quad \hat{P}_k]) \begin{bmatrix} D_{sj}^{-1} & 0 \\ 0 & K_k^{-1} \end{bmatrix}$$

where \hat{U}_j , \hat{T}_j , \hat{Q}_s , \hat{Q}_k , P_s and P_k , are the particular solutions of the equation (1), while S^{-1} , D_{sj}^{-1} and K_k^{-1} are the inverse form of the resulting matrices of global shape functions [9]. Similarly, a contracted expression is found for a cell/solute density defined in equation (3)

$$Gq - Hc = (G\hat{Q} - H\hat{U})F^{-1}(\dot{c} - v \cdot \nabla c + \phi(c)) \quad (7)$$

Here, H and G are the representative matrices of the corresponding boundary element formulation. The columns of F contain values of the global shape function within each discretization point, whereas \hat{C} and \hat{Q} contain the evaluation of the particular solutions \hat{c}_j and \hat{q}_j respectively

$$\nabla^2 \hat{c}_j = f_j \quad (8)$$

On the other hand, new set of global shape functions (equation (??)) for differential analysis into a poroelastic formulation were also implemented to enhance the

numerical approximation of domain integral terms in (??) and (7). Some examples of axisymmetric global functions and particular solutions for diffusive-convective-reactive model are listed below [25]

$$f_j(x, \xi_n) = \frac{2}{\pi} \sum_{v=m_1}^{m_2} L^v \int_0^{\frac{\pi}{2}} (1 - m^2 \sin^2(\varphi))^{\frac{v}{2}} d\varphi \quad (9a)$$

$$\hat{c}_j(x, \xi_n) = \frac{2}{\pi D} \sum_{v=m_1}^{m_2} \frac{L^{v+2}}{(v+2)(v+3)} \int_0^{\frac{\pi}{2}} (1 - m^2 \sin^2(\varphi))^{\frac{v+2}{2}} d\varphi \quad (9b)$$

$$\begin{aligned} \hat{q}_j(x, \xi_n) = & \frac{2}{\pi D} \sum_{v=m_1}^{m_2} \frac{L^{v+2}}{(v+3)} \{ [rn_r + Zn_z] \int_0^{\frac{\pi}{2}} (1 - m^2 \sin^2(\varphi))^{\frac{v}{2}} \\ & + n_r \xi_n \int_0^{\frac{\pi}{2}} (1 - m^2 \sin^2(\varphi))^{\frac{v}{2}} \cos(2\varphi) d\varphi \} \end{aligned} \quad (9c)$$

$$\begin{aligned} Drr = & \sum_{v=m_1}^{m_2} \int_0^{2\pi} \left(-\frac{p_1^{v-2} \beta \xi_n \cos(\varphi) R^2}{k(v+5)} - \frac{p_1^{v-4} \xi_n^2 R^3 v \beta (\sin(\varphi))^2}{k(v+5)} \right) \cos(\varphi) \\ & - \frac{p_1^{v-2} \xi_n R \beta (R \sin(\varphi) - \xi_n) \cos(\varphi)}{k(v+5)} - \frac{p_1^{v-4} \xi_n^2 R^3 v \beta (\sin(\varphi))^3}{k(v+5)} \\ & + \frac{p_1^{v-4} \xi_n^3 R^2 v (\sin(\varphi))^2 \beta}{k(v+5)} + \frac{\beta p_1^{v+2} \cos(\varphi)}{v+2} d\varphi \end{aligned} \quad (10a)$$

$$\begin{aligned} Dzz = & \sum_{v=m_1}^{m_2} \int_0^{2\pi} -\frac{Z \xi_n \cos(\varphi) p_1^{v-2} \beta R}{k(v+5)} - \frac{p_1^{v-4} \xi_n^2 R^2 Z v \beta (\sin(\varphi))^2}{k(v+5)} + \frac{\beta p_1^{v+2}}{v+2} d\varphi \end{aligned} \quad (10b)$$

$$P_r = \frac{\beta}{k} \sum_{v=m_1}^{m_2} \int_0^{2\pi} \beta (\cos(\varphi) R - \xi_n + R \sin(\varphi)) p_1^v d\varphi \quad (10c)$$

$$P_z = \sum_{v=m_1}^{m_2} \int_0^{2\pi} \frac{p_1^{v+2} Z \beta}{k(v+5)(v+2)} d\varphi \quad (10d)$$

where x , ξ_n and $Z = z - Z_n$ are source and field points respectively, p_1 is the distance between them, $L = \sqrt{(R + \xi_n^2)^2 + (z - z_n)^2}$, φ is the angle between vectors defined by source and field, $m = \frac{2\sqrt{R\xi_n}}{L}$, n_r and n_z are the component of outward normal vector at the boundary and $\hat{q}_j(x, \xi_n)$ is the particular solution of fluid flow.

If the field point P is outside the element to be integrated, the integrals of the discrete form of equation (2) are regular and can be numerically computed by implementing the Gauss-Legendre quadrature. However, if the point P coincides with one of the nodes of the integration element, some of the kernels will be singular

and they should be evaluated based on the corresponding singular expansions. The numerical integral associated to these terms must be calculated with a particular quadrature. For example, when dealing with the terms U_{ij}^* and T_{ij}^* , the integration is performed by dividing them into a regular component U_{ij}^{*R} , T_{ij}^{*R} and a singular component U_{ij}^{*W} , T_{ij}^{*W} . For U_{ij}^{*R} and T_{ij}^{*R} a refined numerical integration method and/or an adaptive method (such as Romberg's method or the Gauss-Laguerre quadrature) should be enough.

The numerical integration of the fundamental elastic solution T_{ij}^{*W} , was performed by using an alternative method, based on the combination of two techniques: Rigid Body Motion in Z and Inflation Mode for axisymmetric in r , thus obtaining improper integrals evaluated with high accuracy [11]. In the case where $R = 0$, the above technique is not applied because of restrictions in the collocation-point displacement on the axis of symmetry. The method is applicable to any axisymmetric elastic problem.

Nonlinear behavior is usually related to the reaction term. In spite of the relative roughness, the Newton's method was implemented to compute $F(X) = 0$. The function F is described below:

$$F(X_k) = \left(\frac{M}{\Delta t} + H \right) X_{k+1} - Gq^{k+1} - M\phi(X_{k+1}) - \frac{M}{\Delta t} X_k \quad (11)$$

The Newton scheme for X is:

$$X_{k+1} = X_k + J(X_k)^{-1} F(X_k) \quad (12)$$

where $J(X_k)$ is the Jacobian matrix and

$$X = c(r, z, t_{m+1}) = c^{m+1}$$

$$M = \frac{1}{D}(GQ - HC)$$

For a domain Ω consisting by two regions homogeneous, Ω_1 and Ω_2 respectively as shown in the Figure 1

The boundary of each region ($\partial\Omega$) can be decomposed into Γ_j and Γ_I , with $\Gamma_j \cup \Gamma_I = \partial\Omega_j$, $j = 1, 2$, where Γ_I is the interface between Ω_1 and Ω_2 .

Then the system of equations (7) for each region is given by the equation (13)

$$[H_j H_I] \begin{bmatrix} c_j \\ c_I^j \end{bmatrix} - [G_j G_I] \begin{bmatrix} q_j \\ q_I^j \end{bmatrix} = \begin{bmatrix} d_j \\ d_I^j \end{bmatrix} \quad j = 1, 2. \quad (13)$$

where

$$\begin{bmatrix} d_j \\ d_I^j \end{bmatrix} = \left([H_j H_I] \begin{bmatrix} \hat{C}_j \\ \hat{C}_I^j \end{bmatrix} - [G_j G_I] \begin{bmatrix} \hat{Q}_j \\ \hat{Q}_I^j \end{bmatrix} \right) \begin{bmatrix} F_j \\ F_I^j \end{bmatrix}^{-1} \begin{bmatrix} \hat{b}_j \\ \hat{b}_I^j \end{bmatrix}$$

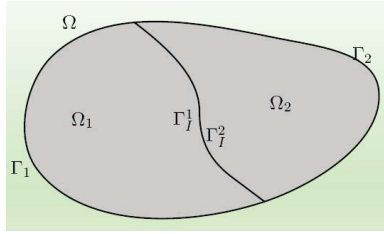


Figure 1: Multi-domain

and

$$\hat{b} = \dot{c} - v \cdot \nabla c + \phi(c) \approx \sum_i \beta_i f_i$$

By the continuity conditions ($c_I^1 = c_I^2 = c_I$) and balance ($q_I^1 = -q_I^2 = q_I$) on the interface Γ_I , we obtain the following system of equations for the domain Ω .

$$\begin{bmatrix} H_1 H_I & 0 \\ 0 & H_I H_2 \end{bmatrix} \begin{bmatrix} c_1 \\ c_I \\ c_2 \end{bmatrix} - \begin{bmatrix} G_1 G_I & 0 \\ 0 & -G_I G_2 \end{bmatrix} \begin{bmatrix} q_1 \\ q_I \\ q_2 \end{bmatrix} = \begin{bmatrix} d_1 \\ d_I \\ d_2 \end{bmatrix} \quad (14)$$

117 Finally applying the boundary conditions on the equation (13) gives a system of
118 equations to be solved.

119 2.2 Numerical implementation

120 This study addresses the understanding of the effects on nutrients concentrations
121 combining several considerations and two models: the quasi-static model present
122 in Mokhbi et al [7] to calculate nutrient concentrations within the intervertebral
123 disc (oxygen, glucose and lactate) via pH level and the model of Ferguson et al [6],
124 where the influence of long-term compression loading on nutrient concentrations
125 was studied.

126 The combined model consisted in an axisymmetric poroelastic model of interver-
127 tebral lumbar-disc, considering four different regions: nucleus (NP), cartilaginous
128 endplates (CEP), outer annulus (OA) and inner annulus (IA), as depicted in Figure
129 2. The dimensions of the disc are 43.5mm diameter, a 12.5mm initial height and a
130 0.5mm CEP thick, according to Ferguson et al [6] and Mokhbi et al [7].

The diffusion equations are coupled by the pH shown in Figure 3 [7]. From equation (3) a set of coupled diffusion-reaction equations yields. The coupling is via pH

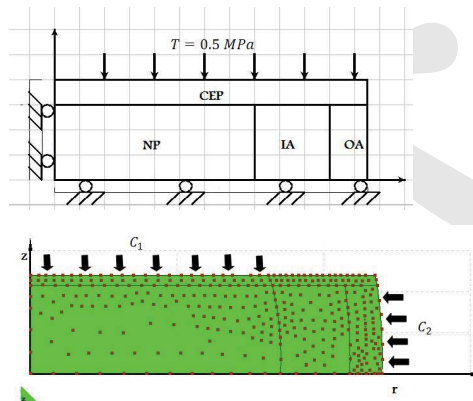


Figure 2: Axisymmetric boundary element model of the intervertebral disc: components and boundary conditions. The parts are: nucleus (NP), inner annulus (IA), outer annulus (OA) and cartilaginous endplate (CEP). Nutrients are provided through the outer annulus and the cartilaginous endplate.

level and lactate/oxygen concentration (see Figure 3).

$$D_{oxi} \nabla^2 c_{O_2} = -F_{O_2cons} + \frac{dc_{O_2}}{dt} \quad (15a)$$

$$D_{lac} \nabla^2 c_{lac} = 2F_{lacpro} + \frac{dc_{lac}}{dt} \quad (15b)$$

$$D_{glu} \nabla^2 c_{glu} = -F_{lacpro} + \frac{dc_{glu}}{dt} \quad (15c)$$

where c_{O_2} , c_{lac} , c_{gluc} are the concentrations of oxygen, lactic-acid and glucose respectively, F_{O_2cons} and F_{lacpro} are the functions that regulate the oxygen consumption and the lactate production. The oxygen consumption depends on the pH and the c_{O_2} , while the lactate production depends on c_{lac} and c_{O_2} (see [29]). Additionally, the energy production is given by glycolysis so that one molecule of glucose is broken into two lactic-acid molecules. Hence the ratio between lactate production and glucose consumption is taken as 2.0 throughout the disc.

Vital nutrients are supplied to the intervertebral disc from the blood vessels located at the boundaries of the disc (Figure 2), while substances transport across the disc is made mainly by diffusion. Both top and bottom boundaries were considered freely permeable, due to the low venous pressure and the highly vascularized nature of the vertebral body. The boundary conditions and the diffusivity within each region are show in Table 1.

The influence of long-term compression loading on nutrient concentration is in-

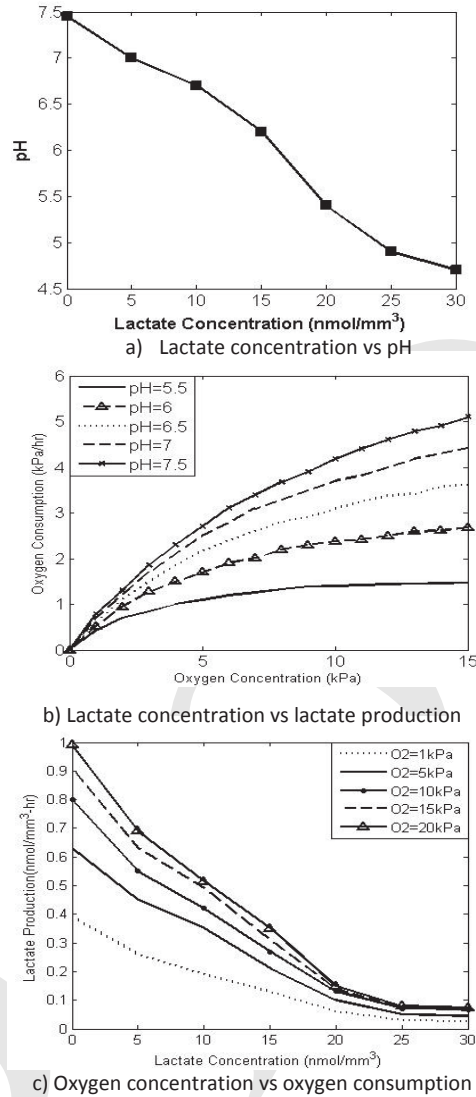


Figure 3: Relationships among pH, oxygen and lactate [7, 29]

investigated by alterations of the geometry and diffusion coefficients as shown in equation (16). A diurnal loading cycle was simulated consisting of two periods: a 16-hours compressive load equivalent to 0.5MPa on the endplate and a final 8-hours period of recovery, simulated with 0.2MPa at the endplate and outer annulus.

Table 1: Disc properties (diffusivity D , boundary concentration C_i , $i = 1$ for the CEP on top of the nucleus, $i = 2$ for the OA periphery, ε is the fluid volume fraction) (from [7]).

	$\varepsilon(\%)$	Cell densities (10^3 cells/mm^3)	Oxygen		Lactic acid		Glucose	
			D mm^2/h	C_i kPa	D mm^2/h	C_i Nmol/mm^3	D mm^2/h	C_i Nmol/mm^3
Nucleus	80	4.0	5.0		2.02		1.36	
IA	73	6.0	4.16		1.68		1.13	
OA	66	12.	3.4	5.8	1.37	0.9	0.92	5.0
CEP	60	15.	2.81	5.1	1.13	0.8	0.76	4.

This resting period was considered to be enough to promote the fluid swelling:

$$D_i = D_i^0 \exp \left(-A \left(\frac{r_i}{\sqrt{kv}} \right)^B \right) \quad (16)$$

144 where i is the solute, r_i is the radius of solute ($r_{O_2} = 0.1\text{nm}$, $r_{lac} = 0.255\text{nm}$ and
 145 $r_{glu} = 3.8\text{nm}$), k is the permeability, v is the water viscosity, D_i^0 is the diffusion (see
 146 Table 1) and A and B are material constants as displayed in Table 2.

Table 2: Disc poroelastic properties (a. [6]; b [30]).

	Elastic modulus ^a	Poisson's ratio ^a	Initialvoid ratio ^a (e_0)	Initial permeability ^a (k_0)	M^a	A^b	B^b
	$E(\text{MPa})$	ν		(m^4/Ns)			
Nucleus	1.5	0.17	4.0	7.5×10^{-16}	8.5	1.25	0.681
Annulus	2.5	0.17	2.33	7.5×10^{-16}	8.5	1.29	0.37
Cartilage	5	0.17	4.0	7.5×10^{-15}	8.5	0	0

An experimental model proposed by Ferguson et al [6] is also implemented to characterize the permeability that depends on phenotype tissues, according to equation (17)

$$k = k_0 \left(\frac{e(1+e_0)}{e_0(1+e)} \right)^2 \exp \left(M \left(\frac{1+e}{1+e_0} - 1 \right) \right) \quad (17)$$

where e is the voids ratio

$$e = \frac{\phi_f}{1 - \phi_f} \quad (18)$$

and ϕ_f is the porosity (fluid fraction) of the tissue as a function of the volume strain $J = dV/dV_0$, as described below

$$\phi_f = 1 - J^{-1}(1 - \phi_0) \quad (19)$$

Table 2 lists model's properties.

3 Numerical Results and Discussion

As mentioned before, the analysis was divided into two periods: a 16-hour period of daily activity where the disc-height loss was continuously calculated and an 8-hour period of fluid re-imbibition where the disc-height is recovered (Figure 4).

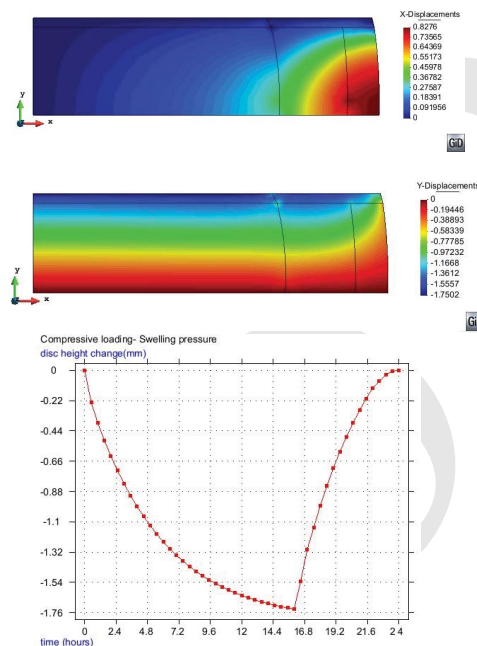


Figure 4: Radial and axial displacements in the intervertebral disc. The disc-height changes during one diurnal loading cycle.

As previously suggested by Mokhbi et al [7] a poor nutrient supply is a potential mechanism for disc degeneration. During the application of the load, the geometry change leads to the transport of substances within the intervertebral disc. However, the compression process also reduces the solute diffusion.

During the loading cycle the disc-height loss corresponding to the 16-hours period was recovered in the swelling phase. This occurs because the fluid re-imbibition during unloading periods runs much faster than the fluid loss (see Figure 4).

The variations in the disc geometry during the loading period facilitate the transport of substances within the disc. Nevertheless this effect involves a reduction in the fluid contents (opposite effect) and thus a reduction of both the solute diffusion and

162 transport. A poor nutrient supply has been suggested as onepotential mechanism
163 for disc degeneration.

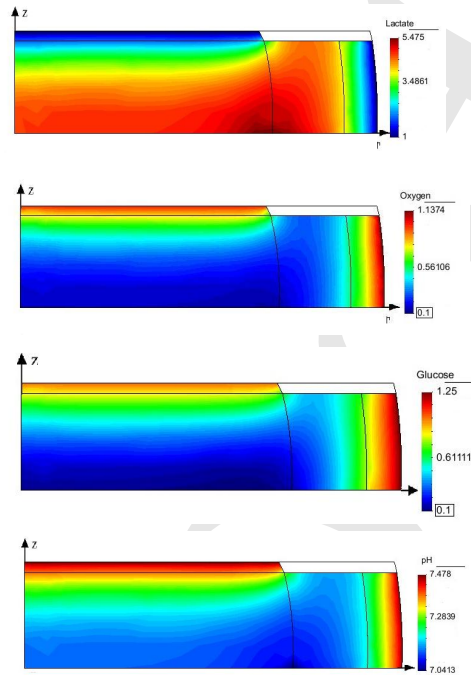


Figure 5: Concentration of lactate [$nmol/mm^2$], oxygen[kPa], glucose [$nmol/mm^2$] and pH for $t = 16h$

164 Both oxygen and glucose concentrations decreased with the distance from the source
165 whereas lactic-acid concentrations were highest in the interface between the nu-
166 cleus and annulus as depicted in Figure 5 and Figure 6. The maximum lactic-
167 acidconcentration ($5.475 nmol/mm^3$) and lowest oxygen concentration ($0.76 kPa$)
168 were found at the same region whereas glucose concentration ($0.56 nmol/mm^3$)
169 occurred at the nucleus (Figure 5 and Figure 6). The variation of the pH was from
170 7.05 to 7.5 throughout the disc.

171 Some endplates fractures (Schmorl's node) produce disruption in the nutrients trans-
172 port. The cell produces a lot of lactic-acid at the center of the disc due to low
173 concentrations of oxygen and glucose present in the disc. Figure 7 shows an in-
174 tervertebral disc with Schmorl's node at the central region of the endplate above
175 the nucleus. The maximum concentrations of lactate were found at the inter-
176 face between the nucleus and inner annulus ($5.7 nmol/mm^3$) and the center of

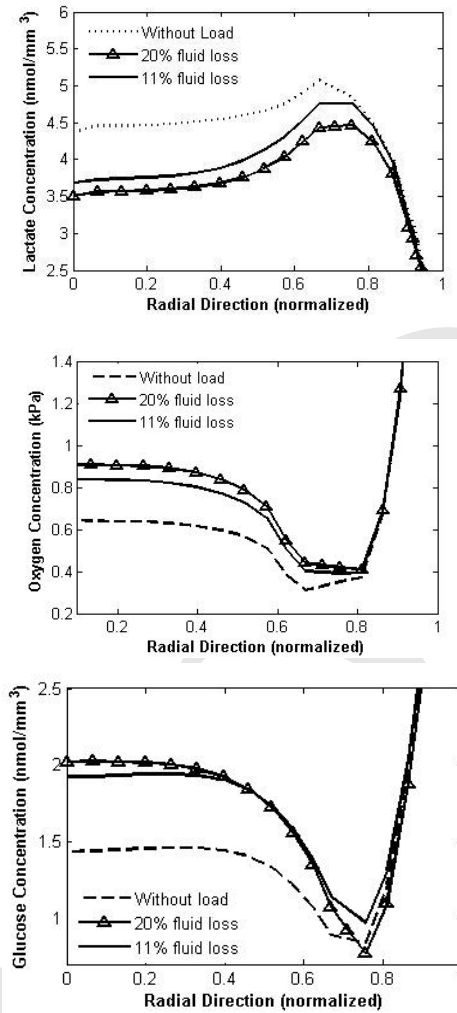


Figure 6: Concentration of lactate [nmol/mm^2], oxygen [kPa] and glucose [nmol/mm^2] in $Z = 0$

the disc ($4.8057 \text{ nmol}/\text{mm}^3$). These locations also exhibit the minimum concentrations of oxygen and glucose (center: 0.09 kPa of oxygen and $1.2538 \text{ nmol}/\text{mm}^3$ of glucose, while at the interface nucleus-annulus: 0.0011 kPa of oxygen and $0.74217 \text{ nmol}/\text{mm}^3$ of glucose).

The ageing and the mechanical environment affects the disc structure and properties and, therefore, the nutrients transport. The nutrients are delivered to the disc

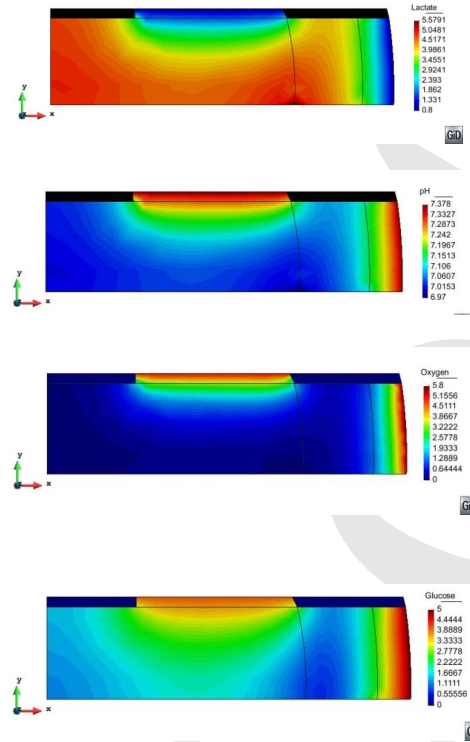


Figure 7: Computed concentrations of lactate [$nmol/mm^3$], oxygen [kPa], glucose [$nmol/mm^3$] and pH for $t = 16h$ in the disc with Schmorl's node at the central region of the endplate above the nucleus.

cells mainly by diffusion since the disc is considered nonvascularized. The disc cell uses oxygen and glucose and produce lactic-acid, thus leading to changes in concentrations that depend on the balance between the rates of transport and cellular activity.

In agreement with the FEM-based model presented by Mokhbi et al (2007), the oxygen and glucose concentrations decreased with the distance from the source at the CEP and OA, while the concentration of lactate increased reaching a maximum close to the nucleus-annulus interface. The maximum computed value was $5.475nmol/mm^3$, while the minimum values of oxygen and glucose concentrations were $0.76 kPa$ and $0.56 nmol/mm^3$ and the minimum pH calculated was 7.05. The simulated central endplates disruption via Schmorl's nodes shown that both oxygen and glucose concentrations fell to very low levels at the disc center below the disturbed area (Figure 7) whereas lactic-acid concentrations increased. It was con-

196 firmed that a poor nutrient supply is a potential mechanism for disc degeneration
197 [30].The values obtained falls within measured ranges and agreed well with the
198 Mokhbi's model and previous works.

199 4 Concluding Marks

200 In this study, a coupled poroelastic and diffusive computer model was implemented
201 using the boundary element method, accounting for multi-domains to predict the
202 influence of the loading disc-height and the transport of the nutrients in the intervertebral
203 disc. This work represents an important contribution in the application of the
204 boundary element method for biological problems. In particular, the ability of the
205 approach for nutrients-diffusion axisymmetric simulation in a poroelastic domain
206 to model the cells behavior in intervertebral discs has been demonstrated.

207 In agreement with Mokhbi's model the oxygen and glucose concentrations decreased
208 with the distance from the source at the CEP and OA, while the concentration
209 of lactate increased reaching a maximum near to the nucleus-annulus interface.
210 The results were in good agreement with those reported in previous works.

211 The multi-domain capability of the code allowed to handle the change of material
212 properties in a simplified manner considering the domain inhomogeneity in a
213 region-by-region way. The nonlinearity of the production/consumption function
214 required large CPU time to obtain the solution. This model incorporates the study
215 of different concentrations of solute at each time instant as well as the influence of
216 the changes in disc shape on the concentrations of oxygen, lactate and glucose that
217 leads to a better simulation of the complex process of nutrients delivery within the
218 intervertebral disc.

219 The need to include moving boundary techniques is an important aspect for future
220 dynamic applications.

221 **Acknowledgement:** The authors gratefully acknowledge the National Council
222 for Scientific Research (CDCH) for the grant number PI-08.7442.2009for funding
223 part of this research. Also, we are indebted to the international project Virtual-
224 Rooms of CIMNE for its support to part of this research.

225 Reference

- 226 [1]Wessel, C., Wrobel, L. & Csilino, A. (2004) *Structural and multidisciplinary*
227 *optimization* **28**, 221–227.
- 228 [2]Gómez, M., García, M., Kuiper, J. & Doblaré, M. (2005) *Theoretical Biology*
229 **235**, 105–119.

- [3]Lu, W., Liu, J. & Zeng, Y. (1998) *Engng Analysis with Boundary Elem* **22**, 167–174.
- [4]Martínez, G., García-Aznar, J., Doblaré, M. & Cerrolaza, M. (2006) *Math & Comp in Simulation* **73**, 183–199.
- [5]Motaghinasab, S., Shirazi-Adl, A., Urban, J. & Parnianpour, M. (2012) *J. of Biomech* **45**, 2195–2202.
- [6]Ferguson, S., Ito, K. & Nolte, L. (2004) *J. of Biomech.* **40**, 213–221.
- [7]Mokhbi, D., Shirazi-Adl, A. & Urban, J. (2007) *J. of Biomech* **40**, 2645–2654.
- [8]Partridge, P., Brebbia, C. & Wrobel, L. (1982) *The Dual Reciprocity Boundary Element Method*. (Computational Mechanics Publications, Boston, USA).
- [9]Park, K. & Banerjee, P. (2007) *Solids and Structures* **44**, 7276–7290.
- [10]Ferragut, L., Asensio, M. & Monero, S. (2007) *Advances in Eng Soft* **38**, 366–371.
- [11]Banerjee, P. (1994) *The boundary element method in engineering*. (McGraw-Hill, UK), 2nd ed edition.
- [12]Beer, G. (2001) *Programming the boundary element method: an introduction for engineers*. (John Wiley, UK).
- [13]González, Y., Cerrolaza, M. & González, C. (2009) *Engineering Analysis with Boundary Elements* **33**, 731–740.
- [14]Galbusera, F., Schmidt, H., Noailly, J., Malandrino, A., Lacroix, D., Wilke, H. & Shirazi-Adl, A. (2011) *Mech. behavior of biomed. mater* **4**, 1234–1241.
- [15]Kima, W., Tretheway, D. & Kohles, S. (2009) *J. of Biomech* **42**, 395–399.
- [16]Yao, H. & Gu, W-Y. (2007) *Journal of Biomechanics* **40**, 2071–2077.
- [17]Zhu, Q., Jackson, A. & Gu, W-Y. (2012) *J. of Biomech* **45**, 2769–2777.
- [18]Hubbard, M. & Byrne, H. (2013) *Theoretical Biology* **316**, 70–89.
- [19]Isaksson, H., vanDonkelaar, C. & Itoa, K. (2009) *J. of Biomech* **42**, 555–564.
- [20]Ochiai, Y. & Takeda, S. (2009) *Engineering Analysis with Boundary Elements* **33**, 168–175.
- [21]Jiang, H. & Yang, B. (2012) *J. of Biomech* **45**, 209–217.
- [22]Haider, M. & Guilak, F. (2007) *Comput. Methods Appl. Mech. Engng* **196**, 2999–3010.
- [23]Checa, S. & Prendergast, P. (2010) *J. Biomech* **43**, 961–968.

- 262 [24]Graciani, E., Mantic, V., Paris, F. & Blazquez, A. (2005) *Comp. & Struc.* **83**,
263 836–855.
- 264 [25]Bai, F. & Lu, Q. (2004) *Engineering Analysis with Boundary Elements* **28**,
265 955–965.
- 266 [26]Biot, M. (1956) *Appl Mech* **78**, 1–6.
- 267 [27]Zerroukat, M., Power, H. & Wrobel, L. (1998) *HeatMass Transfer* **41**, 2429–
268 2436.
- 269 [28]Qiu, Z., Wrobel, L. & Power, H. (1995) *Engng Analysis with BoundaryElem*
270 **15**, 299–312.
- 271 [29]Bibby, S., Jones, D., Ripley, R. & Urban, J. (2005) *Spine* **30**, 487–496.
- 272 [30]Huang, C. & Yong, W. (2008) *J. Biomech* **41**, 1184–1196.